Composite Reinforcement by Magnetic Control of Fiber Density and Orientation

Omri Goldberg,*[ORCID] Israel Greenfeld, and H. Daniel Wagner*

Department of Materials and Interfaces, Weizmann Institute of Science, Rehovot 76100, Israel

S Supporting Information

ABSTRACT: The flexural rigidity of cylindrical specimens, composed of epoxy reinforced by short, magnetized glass fibers, was enhanced using weak magnetic fields (<100 mT). By spatially controlling the magnitude and direction of the field, and thereby the torques and forces acting locally on the fibers, the orientation and concentration of the fillers in the matrix could be tuned prior to curing. Unidirectional alignment of the fibers, achieved using an air-core solenoid, improved the contribution of the fibers to the flexure modulus by a factor of 3. When a ring-shaped permanent magnet was utilized, the glass fibers were migrated preferentially near the rod boundary, and as a result, the contribution of the fibers to the flexure modulus doubled. The fiber length, density, and orientation distributions were extracted by μCT image analysis, allowing comparison of the experimental flexure modulus to a modified rule of mixtures prediction. The ability to magnetically control the fiber distribution in reinforced composites demonstrated in this study may be applied in the fabrication of complex micro- and macroscale structures with spatially variable anisotropy, allowing features such as crack diversion, strengthening of highly loaded regions, as well as economic management of materials and weight.

KEYWORDS: Short-fiber-reinforced polymers, Superparamagnetic iron oxide nanoparticles (SPION), Magnetism, Computed tomography, Flexural rigidity
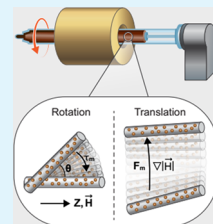
1. INTRODUCTION

The design process of synthetic composites is fundamentally different from the long evolutionary process found in nature. To meet specific mechanical needs, nature relies on structural complexity based on a small number of elements, whereas synthetic composites use a large and diverse array of materials. Natural materials may exhibit different properties when constructed from identical components, thanks to additional degrees of freedom, such as volume fraction and orientation of fibers acting as reinforcing agents.[1] Control over the volume fraction distribution may optimize mechanical functionality by strengthening specific domains with reinforcing fillers. By positioning stiff fibers in regions prone to higher stresses, the mechanical reinforcement may become more effective. Further strengthening may be achieved by control over orientation, taking advantage of the inherent anisotropy of one-dimensional (fibers) and two-dimensional (platelets) fillers, which possess high strength and stiffness along their main axis. Matrix reinforcement by fibers will be isotropic and limited when fiber orientation is random. However, fiber alignment may expand the anisotropy to bulk properties, creating a composite with distinguishable responses in different directions.

The vast collection of available synthetic materials has proven to be useful in diverse composites applications. Nevertheless, the traditional approach lacks structural sophistication and has some inherent drawbacks. For example, the assembly of distinct materials often results in mechanical properties mismatch that may lead to high stress concentrations and failure (delamination).[2] By contrast, integration of compliant and stiff domains within a continuous phase not only enables mechanical tuning but also prevents high stress concentrations at weak interfaces.

Furthermore, uniform dispersion of fillers in a structure is sometimes not optimal in terms of material cost and weight, a drawback that can be overcome by controlling the spatial distribution of filler density and orientation.

There is a growing effort in recent years to prepare intricate structures[3] using methods such as 3D-printing,[4] freeze-casting,[5,6] and mineralization.[7] Particular efforts are directed toward better controlled distribution of particles concentration and orientation, with magnetism standing out as a low-energy, safe, and nondestructive method allowing both features.[8] As magnetic flux density is a vector field, each point in space is characterized by both intensity and direction, where the former may control the filler's spatial volume fraction and the latter its orientation. In order to interact with a magnetic field, the material must have some magnetic compliance quantified by its magnetization. The magnetization direction is governed by the material's alignment relative to an applied magnetic field.

Ferromagnetic and ferrimagnetic materials are characterized by a hysteresis relationship between their magnetization and the applied field, as a result they retain some magnetization after removal of the magnetic source. Paramagnetic materials, on the other hand, do not possess a remnant magnetization; under low fields they have permanent magnetic dipole, and their magnetization (M) scales linearly with the applied magnetic field (H):

$$\vec{M} = \chi \vec{H} \tag{1}$$

A
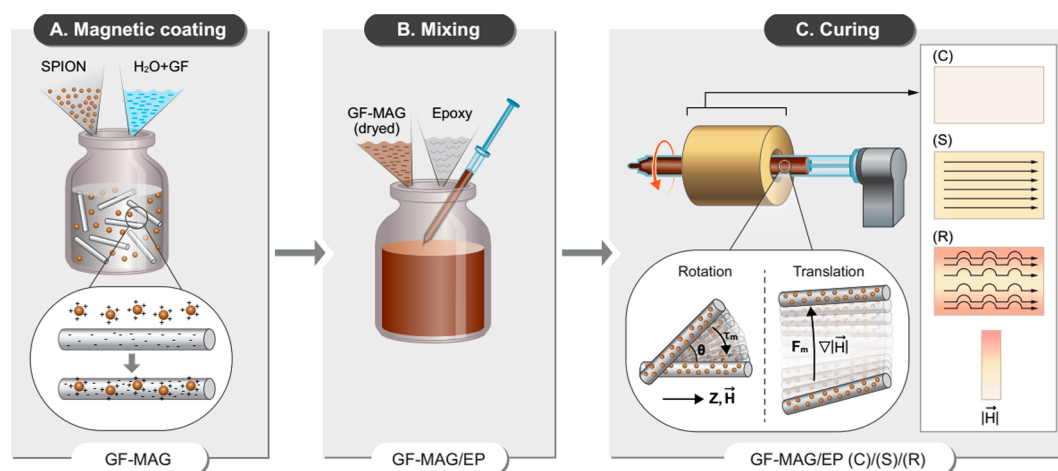
Figure 1. Sample preparation scheme. (A) SPIONs dispersed in cationic ferrofluid adsorbed on pristine glass fibers surface, resulting in brown magnetized fibers (GF-MAG). (B) After drying, the GF-MAG brown powder is mixed in an epoxy resin. Following the addition of a compatible hardener, the GF-MAG/EP mixture is molded inside a cylindrical syringe. (C) The mold is held inside a magnetic source (a solenoid or a permanent magnet) and rotated by a motor while curing. The fibers in the mixture undergo rotation toward the magnetic flux vector ($\vec{H}$) or translation toward the magnetic flux density gradient ($\nabla|\vec{H}|$). In the case of a solenoid (S), the fibers are subjected to a uniform magnetic flux density ($\nabla|\vec{H}|$) with a vector pointing in the z direction, as a result, magnetic torque (τ_m) is acting to minimize their angle with the z axis (θ). In the case of a ring-shaped permanent magnet (R), the fibers are subjected to a nonuniform magnetic intensity with a periodic vector field pattern; consequently, a magnetic force (F_m) is acting on the fibers in the gradient direction toward the mold exterior. Inset: arrows are indicating the magnetic-field lines that represent the vector field along the longitudinal profile of the specimen for a solenoid (S), a ring magnet (R), and in the absence of magnetic source (C). The field-lines spacing indicates the magnetic flux density which is also visualized using a color bar of the magnetic field intensity ($|\vec{H}|$).

where χ is the magnetic susceptibility of the material. The effective value of χ is a function of the material and its geometry.[9] As most common fillers are diamagnetic and therefore carry negative and low susceptibility, they respond only to extremely high magnetic fields, on the order of 10 T, which are impractical for economic use. To orient or translate fillers with lower magnetic fields, they need to be coated with a ferromagnetic or paramagnetic coating.[10] Popular magnetic particles for this use are superparamagnetic iron oxide nanoparticles (SPIONs), which have high magnetic susceptibility.[11,12] Recent studies have demonstrated magnetic alignment using SPION by low magnetic-fields down to values of 8 mT.[13]

Several methods have been suggested over the years for particle alignment, among them are electric-fields, electrospinning, and mechanical stretching.[14−17] Magnetic alignment offers a wide range of achievable torques and is applicable to a spectrum of particle sizes.[8] When a paramagnetic body has geometric anisotropy, the system will minimize its energy by aligning local spins in a manner that nearby atoms work together to increase the internal field.[8] Magnetic translation, on the other hand, is driven by a gradient in the field intensity, therefore, it is not affected by the local field vector and is not restricted to anisotropic particles. The orientation and translation dynamics occur while the medium (matrix) is solidifying under a magnetic field. By the end of the curing process, the system is frozen, and after removal of the magnetic field, the filler particles are trapped in their final state by the solid matrix. Because Brownian motion and gravity are practically negligible, the effect of the magnetic field is restricted only by the damping of the liquid matrix. Due to the gradually increasing viscosity, the minimal field that is required for orientation or translation is limited by the system kinetics. The kinetics can be tuned by setting the applied field, the resin viscosity, the effective susceptibility, and/or the fiber geometry.[18]

Natural evolution overcomes the relative shortage in materials diversity by incorporating structural architectures at a few levels

of hierarchy and thus optimizes the properties according to their local function. Magnetic vector fields may fit that role in the realm of synthetic composites using a new design approach: mapping of stresses developing in a body and transforming them into a corresponding field. Chemical modifications and traditional alignment methods can be used to improve composites strength or stiffness, but they are not suitable to enable intricate spatial control of properties within a continuous phase or to resolve the conflict between strength and toughness.[19]

In this study, two configurations for flexural rigidity optimization were tested on fiber-reinforced cylindrical rod specimens. The first configuration enhanced the flexural rigidity by uniformly aligning the fibers along the rod axis by a solenoid with uniform magnetic field, to increase the fiber orientation efficiency. The second configuration enhanced the flexural rigidity by redistributing the fibers to a favorable geometrical structure with a ring-shaped permanent magnet, to optimize the volume fraction efficiency. While magnetic orientation has been demonstrated in the past,[20,21] our approach suggests the additional and simultaneous control of heterogeneous volume fraction using a spatially designed three-dimensional magnetic field. The proposed method is not restricted to a specific configuration or geometry and may be applied to other stress fields using different magnetic sources.

The common pair of epoxy as a matrix and glass fibers as fillers (GF/EP) served as a model for the present study. Stiffness and strength results of three-point bending tests of both composite rod configurations are then correlated with density and orientation distributions obtained by 3D microcomputed tomography (μCT) imaging. These results are compared with a modified rule of mixture that accounts for the fillers orientation and heterogeneous dispersion.

2. EXPERIMENTAL SECTION

2.1. Magnetic Coating. The composite chosen for the experiments was a short-fiber reinforced composite (SFRP) of epoxy (EP-828,
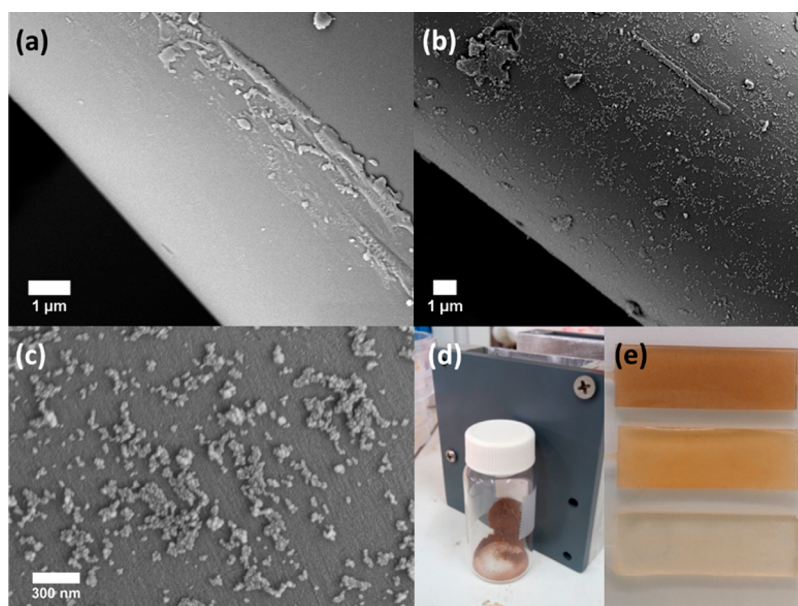
Figure 2. Magnetic decoration of short-fibers. (a) Bare surface of a glass fiber in comparison to (b) magnetically treated fiber. (c) Closeup of 10 nm magnetite nanoparticles on the surface of a magnetically decorated fiber. (d) Magnetically coated glass fibers attracted to a permanent magnet. (e) The change in specimen color as a function of ferrofluid concentration, demonstrated on composites (V_f = 2%) reinforced by fillers treated with concentration of 150 μL/g (top), 50 μL/g (middle), and no-treatment (bottom).

Gvulot, Israel) reinforced with milled E-glass fibers (Microglass-3032, Fibertec Inc.). The short fibers (diameter = 16 μm, average length = 240 μm) were coated with magnetite nanoparticles (diameter = 10 nm, χ = 3.02, saturation magnetization = 22 mT) by adsorption of a cationic ferrofluid (EMG-605, Ferrotech). The ferrofluid was added in a ratio of 150 μL per 1 g of fibers to a vial containing 20 mL of DI water and glass fibers that originally came in white-powder form. The mixture was slowly rotated at 1 rpm for 5 days. The fibers, which by then changed their color from white to brown (Figure 2d, e), were filtered and washed three times. Final drying was done by heating the powder to 110 °C for 5 h.

The attractive force between the cationic surfactant on the nanoparticles and the negatively charged surface of the glass fibers was sufficiently strong to remain stable during the multiple washings and through the entire procedure summarized in Figure 1. The glass fibers were purchased without sizing to allow efficient adsorption of the positively charged nanoparticles directly to the negative oxygen groups of the silica. Although sizing may increase the interfacial adhesion between filler and matrix, it was proved to have negligible effect on the flexure stiffness, the focus of the current study.

2.2. Composite Preparation. Short glass fibers (GF) were mixed in a vial containing epoxy resin (EP) and degassed under vacuum (30 min) to avoid air bubbles. Next, a hardener (EPC-304, Gvulot, Isreal) was added to the mixture (4:10 weight ratio) while gentle manual mixing was performed. After additional degassing of 30 min, the mixture was injected to a 1 mL syringe. Each sample was then cured at room temperature in the presence of its predetermined magnetic conditions while being rotated by a motor to avoid precipitation of the fibers. Three sets of designs were prepared for each volume fraction: random (C), aligned (S), and radial (R). Specimens with random orientation and uniform density were prepared by cross-linking the resin in the absence of a magnetic source. The unidirectional aligned specimens were rotated inside an air-core solenoid (Jantzen-audio, Denmark) inducing a magnetic field of 30 mT along the z direction (Figure 1). The field intensity was determined by correlating it to the supplied current using a Gaussmeter (Lake-shore 460), yielding a solenoid correlation factor of 7.5 mT/A. The "radial" specimens were rotated inside an array of ferromagnetic rings (Or-Pro Magnetic and Promotional Products Ltd., Israel) to obtain a high volume fraction at the rod boundary. After overnight curing, all specimens were postcured inside a furnace at 100 °C for 4 h. Eventually, the syringes were lopped and the composites were

extracted as brown rods with a diameter of 4.2 mm and length of 60 mm. As a reference, the mechanical properties of pristine epoxy (EP) were measured as well.

2.3. Mechanical Measurement. Mechanical properties were measured by performing flexure tests (Instron-5965, 3 mm/min) using a 5 kN load-cell in a three-point bending configuration (span = 41 mm). Each set of measurements was performed using at least eight specimens. The load and displacement in the middle of the rod were recorded by compatible software (Bluehill3). The strength and modulus are spatially varying properties; therefore, for heterogeneous cross sections, as is the case for the radial samples [GF-MAG/EP(R)], they are termed effective, to emphasize the fact that the measurements relate to bulk properties. The formula used for flexural rigidity does not assume a homogeneous cross section and is therefore applicable to a heterogeneous distribution of the volume-fraction as well. The flexural rigidity (bending stiffness, K), effective flexure modulus (E^{eff}), and effective flexure strength (σ^{eff}) were calculated as follows:

$$K = \frac{PL^3}{48\Delta} \tag{2.1}$$

$$E^{eff} = \frac{L^3}{12\pi R^4}\left(\frac{P}{\Delta}\right) \tag{2.2}$$

$$\sigma^{eff} = \frac{L}{\pi R^3}P^{max} \tag{2.3}$$

where P and Δ are the load and the displacement at the middle of the rod, respectively, L is the span, and R is the rod radius. The elastic modulus of the short glass fibers was measured by performing tensile tests on single fibers (Instron-5965, 1 mm/min, gauge length = 80 mm) using a 10 N load-cell and pneumatic gripping. The measurements were performed on continuous fibers identical to their short analogs.

2.4. Microscopy. The dimensions and morphology of the fibers were analyzed by scanning electron microscopy (Supra55, Zeiss). A powder of short glass fibers was scattered over a carbon-tape and coated with a thin layer of Pd/Au (S150 sputter-coater, Edwards). Images were taken with a working distance of 6 mm and an electron energy of 3 keV. Post-testing fractographic images were taken under the same conditions. The distribution of the fibers inside the matrix was evaluated by a microXCT-400 (XRadia, Pleasanton, CA) under working conditions of V = 40 kV and W = 8 W. Raw data were reconstructed with the XRadia
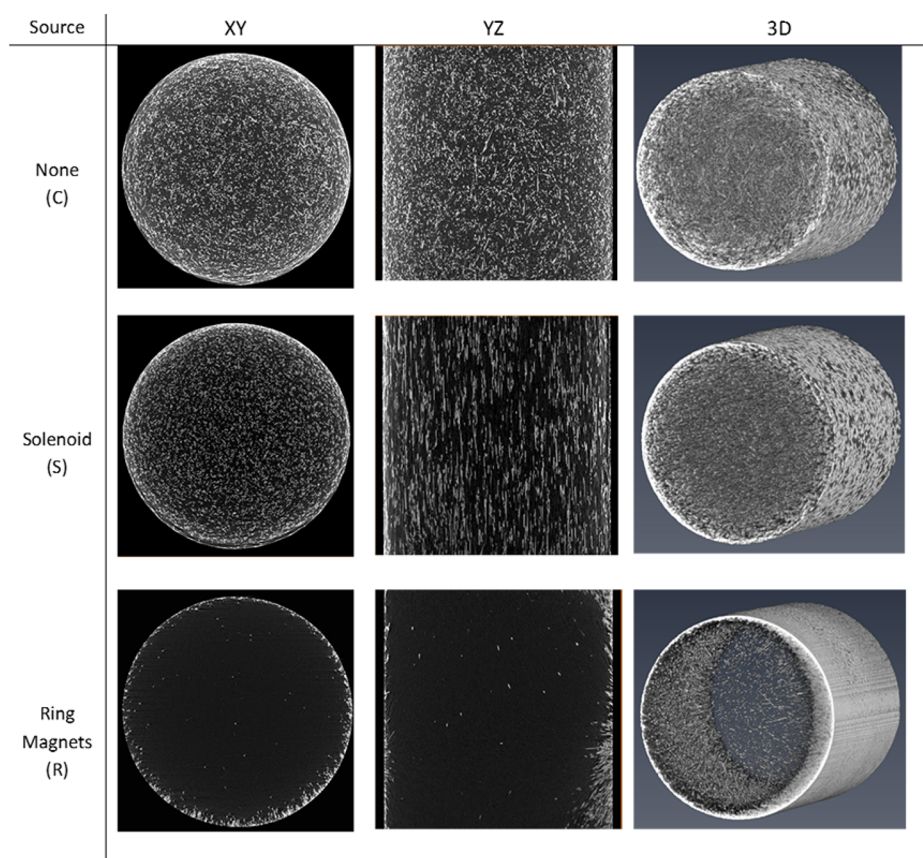
Figure 3. Fibers alignment and concentration. Computed tomography reconstruction of four glass fibers/epoxy composites with a volume fraction of 14%. For each magnetic source, the *XY* cross section (left column), the *YZ* cross section (middle), and the three-dimensional reconstruction are depicted. The composite rod diameter is 4.4 mm.

software, and three-dimensional and ortho-slice visualization was carried out with Avizo software (VSG). Information regarding the distributions of the fibers' length and orientation was retrieved using the cylinder correlation module followed by the "trace correlation lines" tool. Statistics were collected from a representative volume of 2 mm^3 for C and S samples. Specimens cured inside magnetic rings (R) were analyzed using a larger volume of 10 mm^3 due to the heterogeneous nature of the sample.

3. RESULTS AND DISCUSSION

3.1. Magnetic Coating of Short Fibers. SEM images show that the magnetic nanoparticles were successfully adsorbed onto the fibers' surface (Figure 2b,c). Although the weight fraction of the SPIONs relative to the entire decorated fiber was estimated to be less than 10^{-6}, they significantly increased the body's magnetic susceptibility (Figure 2d). Magnetic fields with intensities of less than 100 mT were sufficient to orient and translate the fibers during the curing process in a matter of seconds, which is much shorter than the resin pot-life. Additionally, the SPION adsorption changed the fiber optical response such that the powder's brown color served as an indication of the SPION concentration (Figure 2e). The use of relatively heavy and robust fillers complicated the experimental setup because of gravity effects and caused precipitation. This was resolved by slowly rotating the specimen during the curing process (Figure 1c).

3.2. Mechanical Measurements. We focused on the effect of the magnetic field on the composite microstructure and flexural rigidity; experimental results regarding the flexure modulus (flexural rigidity/second moment of area) of the

composites are summarized in Table 2, and the spatial structure of the different configurations, as reconstructed by computed tomography (μCT), is depicted in Figure 3. The impact of magnetic field on bending strength is depicted in Table 3; however, it is merely discussed in this study. In contrast to stiffness, strength is an extrinsic property that is often controlled by flaws and is therefore widely variable.[22] In the particular case of SFRP, the presence of multiple fiber ends within the composite may result in crack initiation and premature failure.[23] The composite strength may be further improved in future research by optimization of the adsorption process to enable sizing treatment of the fibers prior to magnetic coating.

Control composites were prepared by reinforcement of epoxy with magnetic fibers without the application of a magnetic-field [GF-MAG/EP(C)]. The flexure modulus increased from 3.3 GPa for pristine epoxy to 3.7 and 4.7 GPa for volume fractions of 5% and 14%, respectively. To exclude the effect of the SPIONs on matrix−fiber adhesion and stress transfer performance, the moduli of GF-MAG/EP (composites reinforced by magnetically decorated fibers) and GF/EP (composites reinforced by untreated fibers) were compared in the absence of magnetic field, showing no significant difference. The fibers contributed to the flexure modulus in the absence of magnetic field, whereas the strength of epoxy remained unchanged (at V_f = 5%) and even decreased (at V_f = 14%) upon the addition of pristine glass fibers (Table 3). The addition of magnetically decorated fibers resulted in a decrease in the composite strength for both volume fractions, lowering it by ~15%.

Table 1. Composite Properties

E_m [GPa]	ρ_m [g/cm3]	ν_m	E_f [GPa]	ρ_f [g/cm^3]	$\langle l \rangle$ [μm]	D [μm]
matrix modulus[a]	matrix density	Poisson ratio[b]	fiber modulus[a]	fiber density[c]	fiber length	fiber diameter
3.25 ± 0.12	1.1	0.34	80 ± 12	2.5	240	16

[a]Measured value in flexure (matrix) or tension (fiber). [b]Estimated according to the method of Piggot[22]. [c]Estimated according to the method of ref 28.
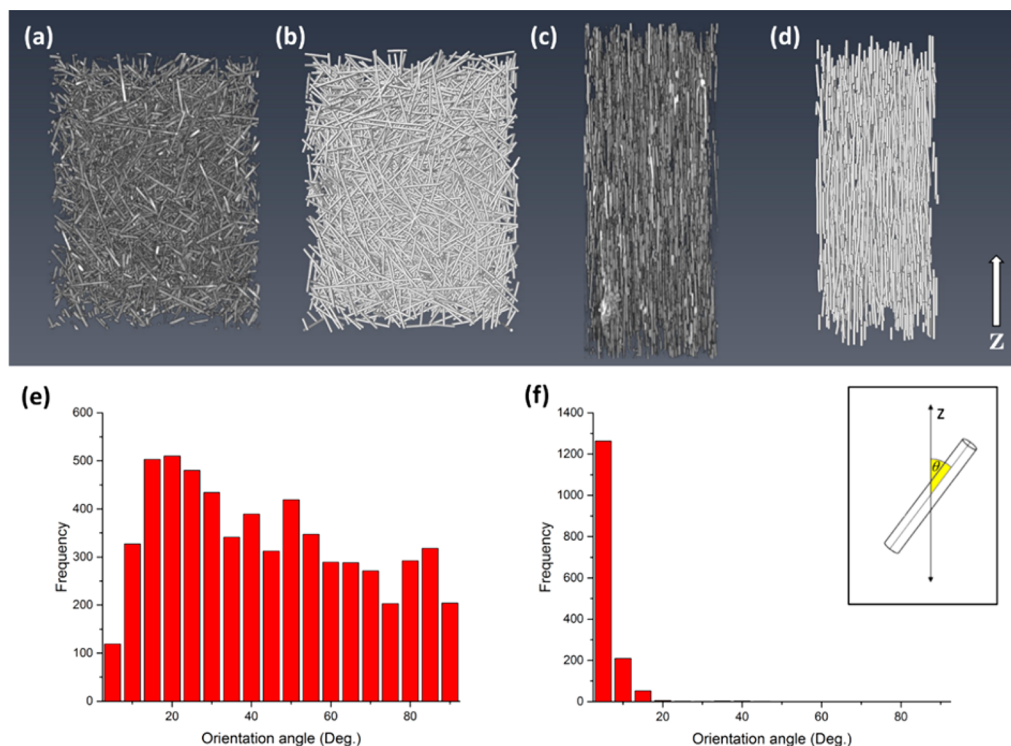
Figure 4. Fibers orientation distribution in rod composites. (a) μCT image of randomly oriented fibers, cured in the absence of magnetic field, and (b) traced correlation lines. (c) μCT image of aligned fibers cured under the influence of a solenoid, and (d) traced correlation lines. (e) Probability density histogram of orientation angles for a control composite in the absence of magnetic field, showing random distribution with some degree of alignment toward the z direction. (f) Probability density histogram of the orientation angles for an aligned composite cured inside a solenoid (orientation control). Inset: definition of the orientation angle θ relative to the strain direction Z.

The contribution of fiber orientation to the flexure modulus was investigated by comparing the control specimens to uniformly aligned fiber composites. To align the glass fibers uniformly, the specimens were cured inside an air-core solenoid inducing uniform and unidirectional magnetic flux along the z direction (Figure 1). μCT images of composites that were cured inside a solenoid [GF-MAG/EP(S)] indicated the uniform distribution of the glass fibers throughout the specimen volume and alignment parallel to the magnetic field vector (Figure 3S). The flexural moduli of aligned composites [GF-MAG/EP(S)] with volume fractions of 5% and 14% were 5.4 and 7.7 GPa, respectively (Table 2).

Flexure tests of the composites that were cured inside an array of ring-magnets [GF-MAG/EP(R)] showed enhanced flexural rigidity, improving the effective modulus of a control specimen with a volume fraction of 5% from 3.7 GPa, when the fibers were randomly and uniformly distributed, to 4.7 GPa, when the fibers were concentrated closer to the external specimen surface. A similar trend was observed for composites with a volume fraction of 14%, as summarized in Table 2. Three dimensional reconstructions of the composite confirmed the radial distribution of the fibers with high concentration near the boundary of the cylinder (Figure 3R).

3.3. Composite Stiffness and Efficiency Factors. Previous studies have addressed the magnetic orientation of particles in composites, mainly of carbon nanotubes (CNTs).[10,24−26] However, the use of magnetized nanotubes in composites is limited to low volume fractions, as they tend to agglomerate, and their scale is the same as their magnetic coating. By contrast, the use of magnetized microfillers is physically different—these particles undergo negligible thermal motion, and the primary relevant forces (excluding the magnetic field) are gravity and damping of the viscous medium. Short-fiber-reinforced polymers (SFRP) are a subclass of fibrous composites that offers rapid and low-cost production, usually by injection molding.[27] The main drive to use SFRPs in the current study was that they are widely used composites, which suffer greatly from the low reinforcement efficiency associated with random orientation. Additionally, microfillers are preferred, since their scale makes them easily visible using μCT imaging, allowing direct measurement of the degree of alignment and volume fraction inside the matrix and monitoring the spatial outcome of experimental variations.

Unlike an ideal system of continuous fibers, short fiber composites do not exploit the full stiffness and strength potential of fibrous material because of the fibers' short lengths and

Table 2. Calculated and Observed Values of Effective Stiffness

		efficiency factors		total efficiency		flexure modulus, E^{eff} [GPa]	
sample[a]	density reinforcement factor, $\chi_d^{cal\,b}$	orientation efficiency factor, $\chi_o^{cal\,c}$	length efficiency factor, $\chi_l^{cal\,c}$	calcd, $\chi_l\chi_o^{cal}$	observed, $\chi_l\chi_o^{obs\,d}$	calcd[e]	observed[e]
EP[f]							3.3 ± 0.1
C (5%)	1	0.42	0.53	0.22	0.16	3.98	3.7 ± 0.2
S (5%)	1	0.99	0.49	0.49	0.59	5.03	5.4 ± 0.4
R (5%)	2	0.40	0.43	0.17	0.22	4.29	4.7 ± 0.2
C (14%)	1	0.37	0.58	0.21	0.18	5.06	4.7 ± 0.3
S (14%)	1	0.99	0.53	0.53	0.47	8.29	7.7 ± 0.6
R (14%)	2	0.40	0.49	0.20	0.21	6.47	6.8 ± 0.2

[a]All samples (except EP) are composites of magnetically decorated glass fibers embedded in epoxy resin. Sample indices are composed by the filler volume fraction (in parentheses) and the magnetic configuration during curing, which is either C (no magnetic source), S (solenoid, orientation control), or R (permanent ring magnet, density control). [b]Density factor equals 1 for uniform spatial distribution or 2 for a thin shell of concentrated fibers at the rod perimeter. For the low volume fractions used in the current study, the deviation from ideal density reinforcement was neglected. [c]Calculated according to eq 4.1 and 4.2 using data collected by computed tomography. [d]Calculated according to eq 5 using measured values from flexure tests. [e]Referring to effective value according to eq 11 (calculated value) or eq 2.2 (observed value). [f]Pristine Epoxy (EP828, Gvulot).
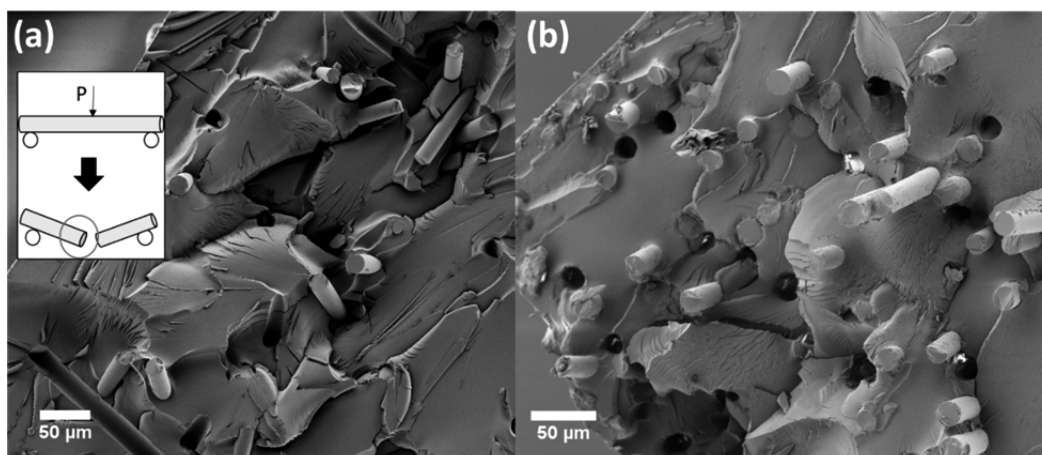
Figure 5. Electron microscope images of a composite rod fracture plane. (a) Randomly oriented pulled-out glass fibers embedded in epoxy. (b) Magnetically aligned (by solenoid) decorated glass fibers embedded in epoxy. Inset: scheme of the fracture plane after three-point bending.

random orientation.[27] In such composites fiber pull-out is the main failure mechanism, generally resulting in improved toughness at the expense of lower contribution to the composite strength and stiffness.[28] The composite stiffness under tension is traditionally modeled using a modified rule of mixture:[22]

$$E = \chi_l\chi_o V_f E_f + (1 - V_f)E_m \qquad (3)$$

where E_f and E_m are the fiber and matrix tensile moduli respectively, V_f is the fiber volume fraction, and χ is an efficiency factor (not to be confused with the magnetic susceptibility) designated by the subscripts l and o for length and orientation, respectively. The product $\chi_l\chi_o$ is regarded as the total reinforcement efficiency of the composite; the loss in reinforcement efficiency due to short length is determined by the fiber dimensions and the matrix–fiber moduli ratio, whereas the orientation efficiency is determined by the unidirectional alignment, which can be improved magnetically. These efficiency factors can be computed according to

$$\chi_l = 1 - \frac{\tanh(ns)}{ns} \qquad n = \sqrt{\frac{2E_m}{E_f(1 + \nu_m)\ln(\pi/V_f)}} \qquad (4.1)$$

$$\chi_o = \sum_{i=1}^{n} f_i \cos^4(\theta_i) = \frac{2}{\pi} \int_0^{\pi/2} f(\theta)\cos^4(\theta) \qquad (4.2)$$

The length efficiency factor χ_l was calculated according to the classic Cox model for short-fiber composites[22,29] using the parameters specified in Table 1, where s is the fiber aspect ratio (length/diameter) and ν_m is the matrix Poisson ratio.

As for the orientation efficiency χ_o, known as the Krenchel factor,[30,31] f_i represents the proportion of fibers having an angle θ_i between their main axes and the alignment vector defined as the strain direction (z in Figure 1c and the inset in Figure 4). Assuming a large population of fibers, the summation of fibers' orientation may be replaced by an integration of the probability density function of the angles $f(\theta)$. For a random distribution in three-dimensions $f(\theta) = \sin(\theta)$ and $\chi_o = 0.2$ and for a random distribution in two-dimensions $f(\theta) = 1$ and $\chi_o = 0.375$.[30] In a full unidirectional alignment $f(\theta) = \delta(0)$, where $\delta(0)$ is an impulse function at $\theta = 0$ and $\chi_o = 1$. Therefore, the alignment can theoretically improve the reinforcement efficiency up to a factor of 5 for perfect alignment.

Expected values of the moduli and efficiency factors were calculated according to the length and orientation distributions as computed using eqs 3, and 4.2. The data regarding the length and orientation distributions were obtained using μCT image analysis (Table 2). The calculated values were compared to observed efficiency factors retrieved from mechanical flexure tests (Table 2) by inverting the modified rule of mixtures (eq 3):

$$\chi_l \chi_o{}^{obs} = \frac{E - E_m(1 - V_f)}{E_f V_f} \tag{5}$$

3.4. Effect of Fiber Orientation on Stiffness. The simplest and most common process to align short fibers is by shear-flow, as per the injection molding technique. However, shear-flow alignment depends on various parameters and often results in a nonuniform orientation distribution.[32]

Parts e and f of Figure 5 depict orientation distribution histograms of $V_f = 5\%$ composites in the absence of magnetic field and under the influence of a solenoid. Orientation efficiency factors were determined for all samples according to eq 4.2, indicating nearly perfect alignment for the composites cured inside the solenoid ($\chi_o > 0.99$). Some degree of alignment in the z direction was consistently observed for all the control composites (no magnetic field, Figure 4e), probably due to the mold anisotropy, leading to a value of $\chi_o = 0.4$, higher than the theoretical value for three-dimensional randomness ($\chi_o = 0.2$).

The effect of the magnetic field on orientation was also observed from SEM images of the fracture surface after the flexure test, indicating unidirectional pull out of fibers in the direction perpendicular to the fracture plane (Figure 5b). By contrast, fracture planes of randomly oriented composites exhibit multidirectional pull-out patterns (Figure 5a).

Control measurements (GF-MAG/EP(C); see Table 2) showed reinforcement of the matrix by the short glass fibers in terms of flexure modulus in spite of their relatively low aspect ratio (length/diameter = ~15) which is lower than the critical aspect-ratio (critical-length/fiber-diameter) typical of GF/EP composites.[22] The combination of subcritical length and random orientation resulted in a poor efficiency factor ($\chi_l \chi_o < 0.2$), as predicted by the theoretical model using the μCT image statistics data (Table 2). Considering that the fiber length distribution remained more or less constant for all specimens (Table 2), the contribution of the orientation efficiency is close to its full potential, as evidenced by the orientation distribution (Figure 4f).

The effect of fiber length on the magnetic orientation was formerly addressed,[33] showing a complicated system of competing negative and positive contributions to the orientation efficiency. Long fibers have higher magnetization, due to the large surface area available for coating, and experience stronger magnetic torques at their edges. Their large surface area also improves stress transfer from the matrix according to eq 4.1. On the other hand, large length may limit orientation by percolation and may lead to high bending stresses and fiber breakage during composite preparation. In this study, we used fiber lengths of about 200 μm, corresponding to an efficiency factor of ~0.5 (Table 2), sufficient for investigating the effects of different magnetic sources. Further investigation of the relations between fiber length and orientation efficiency is beyond the scope of the current study and is deferred for future research.

The experimental results agree well with the modified rule of mixtures predictions (see Table 2 and eq 3), supporting the assumption that orientation and length are key variables of the reinforcement efficiency. Significant improvement in strength was observed for the high volume-fraction composites upon unidirectional alignment, raising it by 60%. A less-dramatic increase (+15%) was observed for the lower volume fraction composites (Table 3). Randomly oriented fibers often interact to constrain matrix flow, causing embrittlement of the composite;[23] thus, the suppression of that mechanism may

Table 3. Bending Stress at Failure

	strength [MPa], $V_f = 5\%$	strength [MPa], $V_f = 14\%$
EP[a]	139.9 ± 2.4	
GF/EP[b]	131.6 ± 11.5	114.4 ± 19.7
GF-MAG/EP(C)[c]	110.2 ± 3.5	95.0 ± 15.4
GF-MAG/EP(S)[c]	126.5 ± 29.8	150.0 ± 18.9
GF-MAG/EP(R)[c]	90.7 ± 8.9	111.4 ± 14.6

[a]Pristine Epoxy (EP828, Gvulot). [b]Composite of epoxy and glass fibers without magnetic decoration. [c]Composites of magnetically decorated glass fibers embedded in epoxy resin. The samples index refer to the magnetic configuration during curing, which is either C (no magnetic source), S (solenoid, orientation control), or R (permanent ring magnet, density control).

explain the substantial increase in strength upon unidirectional alignment.

3.5. Flexural Rigidity of Composites with a Nonuniform Fiber Density. The reinforcement of heterogeneous rods was quantified by analyzing the bending moment of a cylindrical composite possessing a nonuniform volume fraction distribution within its cross section. The effect of nonuniform volume fraction was measured in terms of flexural rigidity which, unlike Young's modulus, is not a material property, as it involves geometry. Flexural rigidity correlates the bending moment with the bending curvature, quite analogously to Hooke's law in tension, where the stiffness correlates the acting force with the displacement. Accordingly:

$$M = -K\kappa \tag{6.1}$$

$$K = \int_A E y^2 \, dA \tag{6.2}$$

here M is the bending moment, K is the flexural rigidity, and κ is the bending curvature ($\kappa = \rho^{-1}$, where ρ is the radius of curvature).[34] The flexural rigidity is calculated by integration of the product Ey^2 along a rod cross section area (A), where y is the vertical distance of each point from the neutral axis. For a homogeneous cross section, E can be taken out of the integral, and the flexural rigidity is simply defined as the product of the flexure modulus and the second moment of area ($K = EI$). For an inhomogeneous cross-section however, K can no longer be decomposed into the product of a material parameter (E) and a pure geometrical parameter (I). Instead, the effects of material and geometry are entangled, and K is calculated according to the spatial distribution of the tensile modulus. By considering the radial distribution of the modulus in polar coordinates, $E(r)$ (assuming axisymmetry):

$$K = \int_0^R \int_0^{2\pi} E(r)(r \sin\theta)^2 r \, d\theta \, dr = \pi \int_0^R E(r) r^3 \, dr \tag{7}$$

where R is the rod radius and r is the radial distance from the rod centerline.

The change in flexural rigidity due to heterogeneous stiffness can be adapted to composite materials by using the modified rule of mixtures, assuming radial distribution of the volume fraction, substituting E from eq 3 into eq 7 and rearranging:

$$K = E_m \left(\chi_l \chi_o \frac{E_f}{E_m} - 1 \right) \left(\pi \int_0^R v_f(r) r^3 \, dr \right) + E_m I \tag{8}$$

where $v_f(r)$ is the *local volume fraction* of an infinitesimal volume element at radial distance r from the rod centerline, and I is the

second moment of area (for a homogeneous cylinder $I = \pi R^4/4$). To clarify the impact of the local volume fraction distribution $v_f(r)$, we defined a dimensionless *density reinforcement factor* (χ_d) by dividing the integral in eq 8 by its solution for a constant volume-fraction:

$$\chi_d = \frac{\pi \int_0^R v_f(r) r^3 \, dr}{\pi \int_0^R V_f r^3 \, dr} = \frac{\pi \int_0^R v_f(r) r^3 \, dr}{I V_f} \tag{9}$$

where V_f, in that case, is the *global volume fraction* computed as the ratio between the total filler volume and the specimen volume:

$$V_f = \frac{2}{R^2} \int_0^R v_f(r) r \, dr \tag{10}$$

The expression for χ_d in eq 9 is only valid under the assumption that the heterogeneous density did not affect the orientation factor χ_o. According to our definition, for an isotropic cross section v_f can be taken out of the integral in eq 9 and $\chi_d = 1$. Accordingly, χ_d is an enhancement factor that is normalized relative to a homogeneous distribution and therefore may be greater than 1.

For a heterogeneous cross section the tensile modulus may not be constant along r. In order to keep the different measurements comparable and consistent, an "*effective modulus*" was defined as the quotient of the flexural rigidity by the second moment of area for a homogeneous cylinder. Inserting χ_d from eq 9 into eq 8 and rearranging, we obtain the effective modulus, which resembles the rule of mixtures in eq 3:

$$E^{eff} = \frac{K}{I} = \chi_l \chi_o \chi_d E_f V_f + (1 - \chi_d V_f) E_m \tag{11}$$

where E^{eff} is the effective modulus measured in units of Pa.

The highest expected value of χ_d can be evaluated by considering a thin layer of filler concentrated at the cylindrical rod boundary (Figure 3R):

$$v_f(r) = \begin{cases} 0 & 0 < r < r_i \\ V_f' & r_i < r < R \end{cases} \tag{12}$$

where V_f' is the local volume fraction of fibers concentrated between some inner diameter r_i and the composite outer diameter R (Figure 6b). Substituting the expression in eq 12 into eq 10 leads to the following relationship:

$$V_f' = \frac{R^2}{R^2 - r_i^2} V_f \tag{13}$$

As a final step, by substituting V_f' for $v_f(r)$ in eq 9 and integrating from r_i to R, the following expression for χ_d is obtained:

$$\chi_d = 1 + \left(\frac{r_i}{R}\right)^2 = 2 - \frac{V_f}{V_f'} \tag{14}$$

which suggests that the optimal reinforcement is achieved, as could be expected, by distributing the fibers in a layer which is as thin as possible $(r_i \approx R)$, resulting in a maximal value of $\chi_d = 2$. Note that for a homogeneous distribution $r_i = 0$ and the solution converges to $\chi_d = 1$. Alternatively, assuming a finite value of V_f' (derived from the fibers packing configuration), χ_d may be expressed by the composite global volume fraction (V_f) using eq 13. Consequently, the right-hand side of eq 14 indicates a linear decrease from the maximal value $\chi_d = 2$ as the global volume
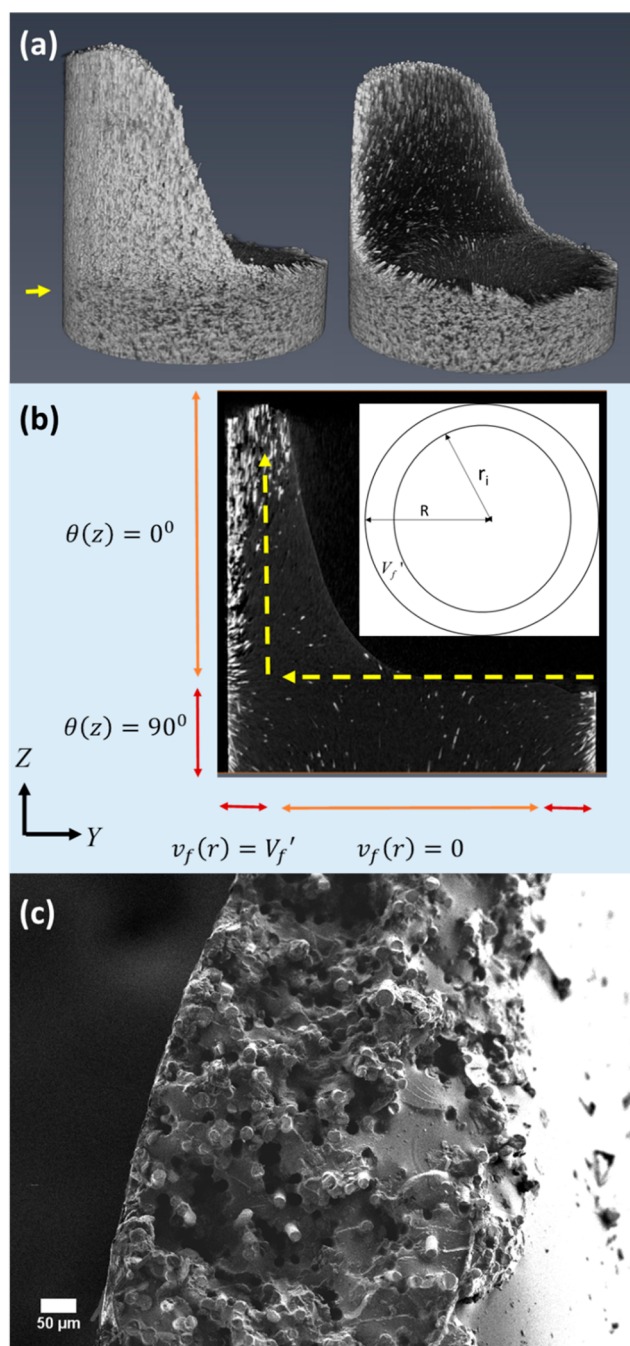
Figure 6. Heterogeneous fiber architecture and crack propagation in a composite rod. (a) Three-dimensional view using computed tomography reconstruction of a postfracture composite cured inside magnetic rings (density control). Transition between two regions characterized by different orientation angles is indicated by an arrow. (b) *YZ* plane view showing the transition from low orientation angles to high orientation angles along the *z* axis and the transition from a fiber-diluted region ($V_f = {\sim}0$) to a concentrated region (local volume fraction V_f') along the radial direction. The dashed arrow indicates the crack trajectory that propagates along the two phase boundaries. Inset: *XY* plane view scheme defining the concentrated region with volume fraction V_f' at a radial distance of $r_i < r < R$. (c) Electron microscope image of the composite fracture plane at the external concentrated shell showing the crack deflection about the concentrated region ($V_f = 5\%$).

fraction increases. However, for the relatively low volume fractions used in the study, that decrease is minor.

An additional way to perceive the density factor χ_d and its effect on the flexural rigidity is by pairing it with the global volume fraction V_f. Referring the product $\chi_d V_f$ in eq 11, we can conclude that the outcome of increasing χ_d is mathematically equivalent to increasing the volume fraction.

For example, a composite with a *global volume fraction* of $V_f = 0.1$, for which its fillers are arranged in a dense thin layer at the cylinder boundary, will possess an *effective volume fraction* of $V_f = 0.2$. In other words, the flexural rigidity of such a composite will be equal to the flexural rigidity of a homogeneous composite with a volume fraction that is twice larger.

3.6. Effect of Fiber Dispersion on Stiffness. To demonstrate the control over the local volume fraction, the resin had to be cured during the application of a different magnetic source, one that induces a field with a spatial intensity gradient. As a primary consideration, the gradient vectors were set to coincide with the desired translation directions of the fillers. Particularly, it is desired to distribute the filler volume fraction to match the stresses acting inside the rod under three-point bending. It is known that the highest contribution to the overall bending stiffness originates from the exterior of a rod, far from the body's center of mass (as manifested in the structure of the bamboo culm for example[35]). Furthermore, as shown in the previous section (eq 14), enhancing the reinforcement at the fiber boundary has the potential to double the flexural rigidity. Correspondingly, the rod cross section structure was optimized to resist bending by concentrating the magnetized fibers at the cylinder perimeter. This was achieved using permanent ring-shaped magnets positioned around the mold during curing and solidifying. Contrary to the solenoid used for unidirectional alignment, the magnetic flux inside the magnetic ring was not uniform, generating a flux gradient along the radial axis of the rod, causing translation of the magnetic fibers toward the rod perimeter (Figure 1c and 3R).

The theoretical predictions were performed by substituting the length and orientation distributions into the model (eq 11). μCT imaging indicated that the fibers were arranged in a periodic orientation pattern that matched the field lines induced by the magnets array. However, the orientation efficiency factors were found to be close to the efficiency factors obtained for the control specimens ($\chi_0 = 0.4$). This observation indicates that the enhanced moduli is a product of an improved volume-fraction distribution. It is seen (Table 2) that the modified rule of mixtures (eq 11) successfully predicts the observed results assuming $\chi_d = 2$. On the other hand, the composites strength seemed to be unaffected by the radial translation of the fibers showing no significant difference relative to GF-MAG/EP(C) (Table 3).

The magnetic configuration used for GF-MAG/EP(R) composites shaped a unique structure that combines a nonuniform concentration distribution along the radial axis and a periodic orientation distribution along the longitudinal axis (Figure 6). Accordingly, the XY cross section can be visualized as a two-phase system: a more diluted phase of lower stiffness where $r < r_i$, and a concentrated phase of higher stiffness where $r > r_i$ (inset in Figure 6b). The longitudinal (z direction) orientation pattern can also be segmented into two phases: longitudinally aligned fibers (low θ) and radially aligned fibers (large θ), sequenced periodically, as visualized in a three-dimensional view of the composite and its YZ cross section (Figure 6). Postfailure analysis of some of the radial specimens indicated a crack propagation trajectory that follows the boundary between the two phases, as observed in the images of the fracture plane

(Figure 6b, c). The periodic orientation pattern that follows the field lines also plays a role in crack propagation, as the crack travels along the boundary of the longitudinal and radial phases. Although quantitative measurements of the periodic specimens' moduli do not provide significant information regarding the properties of such structures, the fact that a spatially controlled field determines the crack propagation trajectory is significant and should be useful in future designs. The method of reinforcement by magnetic control is not restricted to low filler densities; the local volume fraction V_f' of the GF-MAG/EP(R) composites was roughly estimated by electron microscopy to be about 60% for both volume fractions (by substituting $r_i = 0.4$ mm at $V_f = 5\%$ and $r_i = 0.9$ mm at $V_f = 14\%$ in eq 13), indicating that the magnetic control is effective at high volume fractions as well.

4. CONCLUSIONS

Magnetic fiber alignment was adapted to short-fiber composites and was further developed by the use of a magnetic-flux density gradient as a means to translate fillers and control local density. By applying classic beam theory to fibrous composites with heterogeneous filler dispersion, we introduced the concept of effective volume fraction, found to be potentially larger than the fillers' actual total volume fractions. The contribution of glass fibers to the flexural rigidity of epoxy matrix was enhanced by a factor of 3 upon magnetic alignment and by a factor of 2 in the case of optimized density distribution, in good agreement with theoretical predictions. The method can be further generalized to other systems, combining the two strategies of orientation and density control to enhance mechanical properties even more using a proper magnetic source. The control of structural optimization by orientation or translation of fibers can lead to improved performance at lower volume fraction. Apart from these advantages, we demonstrated qualitatively that the short fibers' orientation field can determine the trajectory of a crack during fracture, a potential toughening mechanism through crack diversion or crack-tip shielding adding another dimension to the role of magnetic fields as a tool in materials design.

■ ASSOCIATED CONTENT

ⓢ Supporting Information

The Supporting Information is available free of charge on the ACS Publications website at DOI: 10.1021/acsami.8b02964.

> Three-dimensional and ortho-slice video of a composite cured in the absence of magnetic field [GF-MAG/EP(C)] (MPG)
>
> Three-dimensional and ortho-slice video of a composite cured inside an air-core solenoid [GF-MAG/EP(S)] (MPG)
>
> Three-dimensional and ortho-slice video of a composite cured inside an array of ring-shaped permanent magnets [GF-MAG/EP(R)] (MPG)
>
> Three-dimensional and ortho-slice video of a postfracture specimen cured inside an array of ring-shaped permanent magnets [GFMAG/EP(R)] (MPG)
>
> A list of captions for the videos (PDF)

■ AUTHOR INFORMATION

Corresponding Authors
*O.G. e-mail: omri.goldberg@weizmann.ac.il.
*H.D.W. e-mail: Daniel.Wagner@weizmann.ac.il.
ORCID
Omri Goldberg: 0000-0002-2601-0050

Notes

The authors declare no competing financial interest.

■ REFERENCES

(1) Neville, A. C. *Biology of Fibrous Composites*; Cambridge University, 1993.

(2) Waite, J. H.; Vaccaro, E.; Sun, C.; Lucas, J. M. Elastomeric Gradients: A Hedge Against Stress Concentration in Marine Holdfasts? *Philos. Trans. R. Soc., B* **2002**, *357* (1418), 143−153.

(3) Wegst, U. G. K.; Bai, H.; Saiz, E.; Tomsia, A. P.; Ritchie, R. O. Bioinspired Structural Materials. *Nat. Mater.* **2015**, *14* (1), 23−36.

(4) Kokkinis, D.; Schaffner, M.; Studart, A. R. Multimaterial Magnetically Assisted 3D Printing of Composite Materials. *Nat. Commun.* **2015**, *6*, 8643.

(5) Porter, M. M.; McKittrick, J.; Meyers, M. A. Biomimetic Materials by Freeze Casting. *JOM* **2013**, *65* (6), 720−727.

(6) Porter, M. M.; Yeh, M.; Strawson, J.; Goehring, T.; Lujan, S.; Siripasopsotorn, P.; Meyers, M. A.; McKittrick, J. Magnetic Freeze Casting Inspired by Nature. *Mater. Sci. Eng., A* **2012**, *556*, 741−750.

(7) Mao, L.-B.; Gao, H.-L.; Yao, H.-B.; Liu, L.; Colfen, H.; Liu, G.; Chen, S.-M.; Li, S.-K.; Yan, Y.-X.; Liu, Y.-Y.; Yu, S.-H. Synthetic Nacre by Predesigned Matrix-Directed Mineralization. *Science (Washington, DC, U. S.)* **2016**, *354*, 107−110.

(8) Erb, R. M.; Martin, J. J.; Soheilian, R.; Pan, C.; Barber, J. R. Actuating Soft Matter with Magnetic Torque. *Adv. Funct. Mater.* **2016**, *26*, 3859−3880.

(9) Le Ferrand, H.; Bolisetty, S.; Demirörs, A. F.; Libanori, R.; Studart, A. R.; Mezzenga, R. Magnetic Assembly of Transparent and Conducting Graphene-Based Functional Composites. *Nat. Commun.* **2016**, *7* (May), 12078.

(10) Correa-Duarte, M. a; Grzelczak, M.; Salgueirio-Maceira, V.; Liz-Marzan, L. M.; Farle, M.; Sierazdki, K.; Diaz, R.; Giersig, M.; Liz-marza, L. M. Alignment of Carbon Nanotubes under Low Magnetic Fields through Attachment of Magnetic Nanoparticles. *J. Phys. Chem. B* **2005**, *109*, 19060−19063.

(11) Wang, X.; Zhao, Z.; Qu, J.; Wang, Z.; Qiu, J. Fabrication and Characterization of Magnetic Fe_3O_4-CNT Composites. *J. Phys. Chem. Solids* **2010**, *71* (4), 673−676.

(12) Laurent, S.; Forge, D.; Port, M.; Roch, A.; Robic, C.; Vander Elst, L.; Muller, R. N. Magnetic Iron Oxide Nanoparticles: Synthesis, Stabilization, Vectorization, Physicochemical Characterizations and Biological Applications. *Chem. Rev.* **2008**, *108* (6), 2064−2110.

(13) Erb, R. M.; Libanori, R.; Rothfuchs, N.; Studart, a. R. Composites Reinforced in Three Dimensions by Using Low Magnetic Fields. *Science (Washington, DC, U. S.)* **2012**, *335* (6065), 199−204.

(14) Xie, X. L.; Mai, Y. W.; Zhou, X. P. Dispersion and Alignment of Carbon Nanotubes in Polymer Matrix: A Review. *Mater. Sci. Eng., R* **2005**, *49* (4), 89−112.

(15) Frogley, M.; Ravich, D.; Wagner, H. D. Mechanical Properties of Carbon Nanoparticle-Reinforced Elastomers. *Compos. Sci. Technol.* **2003**, *63* (11), 1647−1654.

(16) Frogley, M.; Zhao, Q.; Wagner, H. D. Polarized Resonance Raman Spectroscopy of Single-Wall Carbon Nanotubes within a Polymer under Strain. *Phys. Rev. B: Condens. Matter Mater. Phys.* **2002**, *65* (11), 113413.

(17) Frogley, M. D.; Wagner, H. D. Mechanical Alignment of Quasi-One-Dimensional Nanoparticles. *J. Nanosci. Nanotechnol.* **2002**, *2* (5), 517−521.

(18) Erb, R. M.; Segmehl, J.; Charilaou, M.; Löffler, J. F.; Studart, A. R. Non-Linear Alignment Dynamics in Suspensions of Platelets under Rotating Magnetic Fields. *Soft Matter* **2012**, *8* (29), 7604.

(19) Ritchie, R. O. The Conflicts between Strength and Toughness. *Nat. Mater.* **2011**, *10* (11), 817−822.

(20) Martin, J. J.; Fiore, B. E.; Erb, R. M. Designing Bioinspired Composite Reinforcement Architectures via 3D Magnetic Printing. *Nat. Commun.* **2015**, *6*, 1−7.

(21) Le Ferrand, H.; Bouville, F.; Niebel, T. P.; Studart, A. R. Magnetically Assisted Slip Casting of Bioinspired Heterogeneous Composites. *Nat. Mater.* **2015**, *14*, 1172−1179.

(22) Piggott, M. R. *Load Bearing Fibre Composites*, 2nd ed.; Kluwer Academic Publishers, 2002.

(23) Kim, J.-K.; Mai, Y.-W. High Strength, High Fracture Toughness Fibre Composites with Interface Control - A Review. *Compos. Sci. Technol.* **1991**, *41*, 333−378.

(24) Prolongo, S. G.; Meliton, B. G.; Del Rosario, G.; Ureña, A. New Alignment Procedure of Magnetite-CNT Hybrid Nanofillers on Epoxy Bulk Resin with Permanent Magnets. *Composites, Part B* **2013**, *46*, 166−172.

(25) Ma, C.; Liu, H.-Y.; Du, X.; Mach, L.; Xu, F.; Mai, Y.-W. Fracture Resistance, Thermal and Electrical Properties of Epoxy Composites Containing Aligned Carbon Nanotubes by Low Magnetic Field. *Compos. Sci. Technol.* **2015**, *114*, 126−135.

(26) Shi, D.; He, P.; Zhao, P.; Guo, F. F.; Wang, F.; Huth, C.; Chaud, X.; Bud'Ko, S. L.; Lian, J. Magnetic Alignment of Ni/Co-Coated Carbon Nanotubes in Polystyrene Composites. *Composites, Part B* **2011**, *42* (6), 1532−1538.

(27) Fu, S. Y.; Lauke, B. Effects of Fiber Length and Fiber Orientation Distributions on the Tensile Strength of Short-Fiber-Reinforced Polymers. *Compos. Sci. Technol.* **1996**, *56* (10), 1179−1190.

(28) Hull, D.; Clyne, T. *An Introduction to Composite Materials*; Cambridge University Press, 1996.

(29) Cox, H. L. The Elasticity and Strength of Paper and Other Fibrous Materials. *Br. J. Appl. Phys.* **1952**, *3*, 72.

(30) Krenchel, H. *Fibre Reinforcement; Theoretical and Practical Investigations of the Elasticity and Strength of Fibre-Reinforced Materials*; Akademisk Forlag: Copenhagen, 1964.

(31) Eichhorn, S. J.; Young, R. J. The Young's Modulus of a Microcrystalline Cellulose. *Cellulose* **2001**, *8* (3), 197−207.

(32) Gupta, M.; Wang, K. K. Fiber Orientation and Mechanical Properties of Short Fiber Reinforced Injection Molded Composites: Simulated and Experimental Results. *Polym. Compos.* **1993**, *14* (5), 367−382.

(33) Ciambella, J.; Stanier, D. C.; Rahatekar, S. S. Magnetic Alignment of Short Carbon Fibres in Curing Composites. *Composites, Part B* **2017**, *109*, 129−137.

(34) Bauchau, O. A.; Craig, J. I. *Structural Analysis: With Applications to Aerospace Structures*; Springer, 2009; Vol. 53.

(35) Nogata, F.; Takahashi, H. Intelligent Functionally Graded Material: Bamboo. *Compos. Eng.* **1995**, *5* (7), 743−751.